Korean J. Chem. Eng., 36(3), 478-488 (2019)
DOI: 10.1007/s11814-018-0221-7

pISSN: 0256-1115
eISSN: 1975-7220

Effects of montmorillonite on the enhancement of physicochemical, optical and photocatalytic properties of TiO_2/chitosan bilayer photocatalyst

Noor Nazihah Bahrudin† and Mohd Asri Nawi

School of Chemical Sciences, Universiti Sains Malaysia, 11800 Minden, Penang, Malaysia
(*Received 30 August 2018 • accepted 27 December 2018*)

Abstract−Chitosan-montmorillonite (CS-MT) composites of different MT composition were prepared in 5% of acetic acid solution and fabricated on glass plates. The composite film was then combined with TiO_2 in an immobilized layer-layer manner for removing methyl orange dye via synergistic photocatalytic-adsorption processes. The effects of MT addition to the CS matrix were investigated with respect to the physicochemical and optical properties. The presence of MT within the composite reduced the swelling and improved the adhesiveness as well as the thermal stability of CS. The MT clay assisted in producing higher hydroxyl radicals and improving the solid-state oxidation of CS within the adsorbent sub-layer for the photocatalytic enhancement of TiO_2/CS-MT than its counterpart TiO_2/CS. Subsequently, the photocatalytic activity of the TiO_2/CS-MT was 1.3 and 4.2-times better than the TiO_2/CS and TiO_2 photocatalysts, respectively. This TiO_2/CS-MT photocatalyst was also reusable for at least ten cycles of application.

Keywords: Chitosan-montmorillonite, Electron-hole Separation, Optical Properties, Photocatalytic Oxidation, Physicochemical Enhancement

INTRODUCTION

Titanium dioxide (TiO_2) is a well-received photocatalyst in environmental remediation for its inertness, long-term photostability and being less likely to produce secondary pollutant [1,2]. TiO_2 can oxidize organic and inorganic substances through a redox reaction for potential application in the homogeneous and heterogeneous catalysis [1,3]. The photocatalytic activity of TiO_2 is practically related to the quantity of reactants adsorbed on the photocatalyst's surface [4]. Hence, TiO_2 can be combined with different types of adsorbents such as polymers [5,6] or clays [7,8] to increase the specific surface area as well as the contact with the contaminants. The combination can also enhance the photocatalytic activity of the composites as the charge separation and visible-light responsive can be potentially induced [4].

Chitosan (CS) is a biodegradable polymer which can function as adhesive with the ability to form film [9]. Similarly, montmorillonite (MT), a clay mineral, is a valuable material due to its large surface area, good cation exchange capacity (CEC) and layer expansion capacity, as well as being inexpensive, environmentally benign and rich in reserve [10,11]. However, some related issues have been identified for aqueous applications where CS exhibits poor mechanical strength and high solubility in the acidic media, while MT clay has a strong interaction with water, which results in its hardness, flocculation and dispersion when in an aqueous medium [12]. The combination of CS and MT as a composite adsorbent can be considered mutual, as the advantages and drawbacks of each material can be either combined or eliminated for application in the environmental clean-up [6,13,14]. Thus, the CS-MT composite adsorbent becomes more robust and can be used to adsorb many anionic organic dyes since higher removal efficiency can be achieved than the individual materials. The abundantly available -OH groups of CS can form hydrogen bonds with the Si-O-Si groups of silicate of MT [15]. Therefore, good adsorption properties of anions are obtained as most of the protonated $-NH_3^+$ groups on the CS backbone are not directly interacting with the clay surface [16]. For the photocatalysis application, the TiO_2/CS can enlarge the specific surface area [17] and has shown some interesting mechanisms such as charge transfer [14,18] and solid-state oxidation [19-21] besides improving the photocatalytic properties of TiO_2. Meanwhile, the coupling of MT clay with TiO_2 can enhance the optical properties of the composite by shortening the length of charge transport and enabling efficient charge separation to improve the photocatalytic activity [22]. For instance, Chen et al. synthesized TiO_2 pillared MT clay with improved porosity, surface area and photocatalytic activity [23]. Similarly, Yuan et al. [8], Zhang et al. [24] and Dou et al. [25] synthesized TiO_2/MT nanocomposites by different methods and observed the improvement in the photocatalytic activity more than the individual materials.

Despite numerous publications on the composite of TiO_2/CS and TiO_2/MT as seen in Table 1, only Vijayalekshmi [26] reported on the TiO_2/CS-MT combination by different preparation method and focused on the antibacterial properties of the composite. With that as motivation, we fabricated the CS-MT composite as the adsorbent sub-layer of TiO_2 via the immobilized bilayer assemblage to decolorize methyl orange (MO) dye as the probe pollutant. We believe that this type of assemblage is a simple way of making TiO_2/CS-MT, a photocatalyst without altering the TiO_2 crystallite and

†To whom correspondence should be addressed.
E-mail: nazihah.noor@yahoo.com

Table 1. Comparison of TiO_2/CS, TiO_2/MT and TiO_2/CS-MT photocatalysts, their applications and properties enhancement

Photocatalysts	Combination modes	Target substrate	Applications	Properties enhancement	Ref.
TiO_2/CS	Layer by layer dip-coating	Phenol	Wastewater treatment	Generate highly porous TiO_2, reduce recombination of electron-hole pairs and improve photocatalytic activity by two times.	[9]
TiO_2/CS	TiO_2 was coated on CS coating layer	Thymol violet, *E. coli* bacteria	Wastewater treatment, Antibacterial	Large surface area and bacterial inhibitive effect.	[17]
TiO_2/CS	TiO_2-CS emulsion coated on the squared glass plate	Pathogenic microbes	Food packaging	High tensile strength, wettability, low transmittance, protect microbial infection and extend shelf life of fruit.	[47]
TiO_2/CS	TiO_2-CS was coated on Al electrode	Aluminium metal	Anti-corrosion	Form protective layer and suppress anodic corrosion.	[48]
TiO_2/MT	TiO_2 dispersed on MT	Methyl orange	Wastewater treatment	Large surface area, pore size and pore volume, no aggregation between TiO_2 and MT, and 10% photocatalytic improvement.	[8]
TiO_2/MT	Layer by layer dip-coating	Methylene blue dye	Wastewater treatment	Redshift in absorption wavelength, low recombination rate of electron-hole pairs and low band gap energy.	[7]
TiO_2/MT	Acid catalyzed sol-gel	CO_2	CO_2 reduction	Small particle size, large surface area, reduce band gap energy and reduce recombination of electron-hole pairs.	[22]
TiO_2/MT	TiO_2 dispersed on MT	2,4-dichlorophenol	Wastewater treatment	High specific surface area, pore size and pore volume and high degradation efficiency.	[24]
TiO_2/MT	Hydration of TiO_2/MT	General	General	Small crystallite size, high phase change temperature for anatase-rutile transformation.	[49]
TiO_2/MT	Hydrolysis of TiO_2/MT	General	General	Large surface area, pore volume, small particle size.	[50]
TiO_2/CS-MT	Mixing of CS, MT and TiO_2	Gram negative and positive bacteria	Antibacterial	High tensile strength and modulus elongation; Reduce band gap energy; High bacterial activity.	[26]
TiO_2/CS-MT	Layer by layer dip-coating	Methyl orange	Wastewater treatment	High adhesiveness; Improve thermal stability; Reduce swelling and band gap energy; Improve hydroxyl radicals production.	This study

hindering the aggregation of TiO_2 particles during the interaction with CS-MT. In addition, the dominant layer and the role of each material of the photocatalyst can be identified easily [7,27,28]. For this study, we focused on the effects of adding MT clay in enhancing the physicochemical properties of CS adsorbent sub-layer composite as well as the optical properties of this TiO_2/CS-MT photocatalyst. The physicochemical investigations involved the adhesion strength, swelling surface morphology and thermal stability analyses of CS-MT sub-layer, while the optical properties of TiO_2/CS-MT were checked via ultraviolet-visible diffuse reflectance spectrophotometer (UV-vis DRS) and fluorescence spectrophotometer (FLS) analyses. Finally, the photocatalytic enhancement of TiO_2/CS in the presence of MT was observed under UV-vis and total visible light irradiations.

MATERIALS AND METHODS

1. Materials

Chitosan flakes (CS; MW: 322 g mol^{-1}), montmorillonite powder (MT, K-10) and terephthalic acid (TA) were purchased from Sigma-Aldrich. Glacial acetic acid (99.8%) was bought from System® while TiO_2 Aeroxide® (TiO_2; 80% anatase, 20% rutile) was purchased from Jebsen & Jessen Degussa Chemicals (M) Sdn. Bhd. Epoxidized natural rubber with 50% mole of epoxidation (ENR) and polyvinyl chloride (PVC) powder were obtained from Guthrie Group Sdn. Bhd. and Petrochemical (M) Sdn. Bhd., respectively. Toluene (C_7H_8) and dichloromethane (CH_2Cl_2) were bought from R & M Chemicals prior for ENR and PVC dissolution, respectively. ENR was refluxed in 250 mL toluene at 88-90 °C to obtain a

ca.~11.3% (w/v) viscous solution. Methyl orange dye from BDH Chemicals Ltd. (MO; color index no=C.I 13025, MW: 327.33 g mol^{-1}, molecular formula: $C_{14}H_{14}N_3NaO_3S$) was selected as the model pollutant. Ultra-pure water (UPW, 18 MΩ cm^{-1}) was used for solution and dilution purposes.

2. Fabrication of TiO_2/CS-MT and TiO_2/CS

To determine the optimum MT, different percentage of MT (0, 12, 24, 33, 50%) was each, mixed with a fixed amount of CS powder and dissolved in 50 mL of 5% (v/v) of acetic acid solution using a ball mill grinder at a speed of 40 rpm for 6 h. The solutions were cast directly on the glass plates with dimensions of 4.5 cm×7.0 cm×0.2 cm and left to dry at room temperature for an overnight before drying in the oven for the next 48 h at 60 °C. For the TiO_2 dip-coating formulation, 6 g of TiO_2 powder in a mixture of ENR/C_7H_8 and PVC/CH_2Cl_2 adhesive blend was sonicated until a homogeneous formulation was obtained [29]. The dried CS-MT adsorbent plate was dip-coated in the TiO_2 formulation in a coating cell for desired loadings as determined by weighing the CS-MT plate and final weight of the TiO_2 coated plate. The TiO_2/CS plate was also prepared using the same method.

3. Physicochemical and Optical Characterizations

For adhesion test, the CS-MT plates with a fixed loading of 1.27 mg cm^{-2} were prepared from the casting solutions of different MT composition. Each plate was put in a beaker containing water and sonicated in an ultrasonic bath for 5 s, dried in the oven and weighed. The steps were repeated until 30 s [30]. The swelling test was carried out according to a method reported by Wan et al. [31], in which the test was done for different CS:MT composition ratio plate and pH adjusted solution. The adhesiveness and swelling ratio of the polymer adsorbents are calculated using the following equations:

$$\text{Adhesiveness}\ (\%) = \frac{(W_1 - W_2)}{m} \times 100 \quad (1)$$

$$\text{Swelling ratio}\ (\%) = \frac{(W_s - W_d)}{m} \times 100 \quad (2)$$

where W_1 is the initial weight of the coated plate, W_2 is the weight of the plate after 30 seconds, m is the initial weight of the immobilized adsorbent on the plate, W_s is the weight of the swollen sample (g) and W_d is the weight of the dried sample.

The morphologies of the CS and CS-MT composites were captured under scanning electron microscopy (SEM) (LEO Supra 50 VP), and transmission electron microscopy (TEM) analysis was conducted using a high-resolution TEM (JEM-2100 F, JEOL). A thermogravimetric analyzer (TGA) (STAR e3.2, TA Instruments) was used to conduct the TGA analysis conditioned with a heating rate of 10 °C min^{-1} and scanned from 30 °C to 920 °C under inert N_2 gas flow. For the UV-visible diffuse reflectance analysis, it was performed on a UV-vis diffuse reflectance spectrophotometer (Lambda 35, Perkin Elmer) within 200-600 nm scan range using a magnesium oxide (MgO) disc as the reflectance standard. The produced hydroxyl radicals were detected using a fluorescence spectrophotometer (LS-55, Perkin Elmer) at λ_{ex} of 315 nm following a method by Sabri et al. [32]. Only the TGA analysis used the samples which were peeled off from the plates and ground, while other analyses characterized the samples in their immobilized form.

4. Adsorption and Photocatalytic Oxidation Set-up

For all experiments, the adsorbent and photocatalyst plates were vertically put in a glass cell (length, 5.0 cm; width, 1.0 cm and height, 8.0 cm) containing 20 mL of 20 mg L^{-1} MO solution, respectively. The adsorption proceeded in a sealed box, while for the photocatalytic oxidation experiment, the cell without the box was placed in front of a 45-W home fluorescent lamp in which the coated area of the plate faced the lamp. The UV leakage of the lamp was 2.78 W m^{-2} as measured by a radiometer (solar light co. PMA 2100) connected with UV-A and UV-B broadband detectors (PMA 2107). Aeration with a flow rate of 40 mL min^{-1} was constantly supplied from an aquarium pump connected to the reactor with a PVC tubing. The absorbance of the treated dye was measured by a direct spectrophotometer (Model DR/2000) from HACH at 464 nm. The removal efficiency (R) of MO was calculated using the following equation;

$$R\ (\%) = \frac{(C_o - C_e)}{C_o} \times 100 \quad (3)$$

Here, C_o is the initial concentration of the dye and C_e is the concentration of the dye at equilibrium in mg L^{-1}.

5. Generation of the Porous Photocatalyst

The photocatalytic improvement of TiO_2/CS-MT photocatalyst was done by generating a porous TiO_2 surface via photo-etching. This method has been used to generate porous TiO_2/crosslinked-CS [20,21], and modified TiO_2 [32] as the macropores were created within TiO_2 after ENR had been degraded. The porous TiO_2/CS-MT surface was obtained after the ENR degradation had ceased as denoted by zero TOC value. In the photo-etching experiment, the optimized TiO_2/CS-MT plate was irradiated in 20 mL of ultrapure water, whereby at every time interval a water sample was collected for the TOC analysis and the remaining water was changed with the new volume for the subsequent cycle until it reached 12 h. The single TiO_2 plate was also prepared for a comparison purpose. The pseudo-first-order rate constant, k (min^{-1}), was calculated using the linearized Langmuir Hinshelwood equation.

$$\ln\left(\frac{C_o}{C_t}\right) = kt \quad (4)$$

where C_t is the concentration of MO dye (mg L^{-1}) at time, t.

RESULTS AND DISCUSSION

1. Physicochemical Characterizations

The combination of MT clay with CS can change the polymer structure as well as the physicochemical properties due to the interaction with the hydroxyl and amino groups of CS [33]. Thus, the MT composition of 0% (CS only), 12%, 24%, 33% and 50% within the CS-MT casting solution was investigated by means of MO removal, adhesiveness and swelling properties as shown in Fig. 1(a). On the other hand, Fig. 1(b) shows the swelling ratio of the optimum immobilized CS-MT composite in different pH of the ultrapure water to see its behavior in different pH solution.

Fig. 1(a) illustrates that the highest removal of MO was achieved when the immobilized adsorbent was prepared from 12% of MT composition in the casting solution. This was followed by the poly-

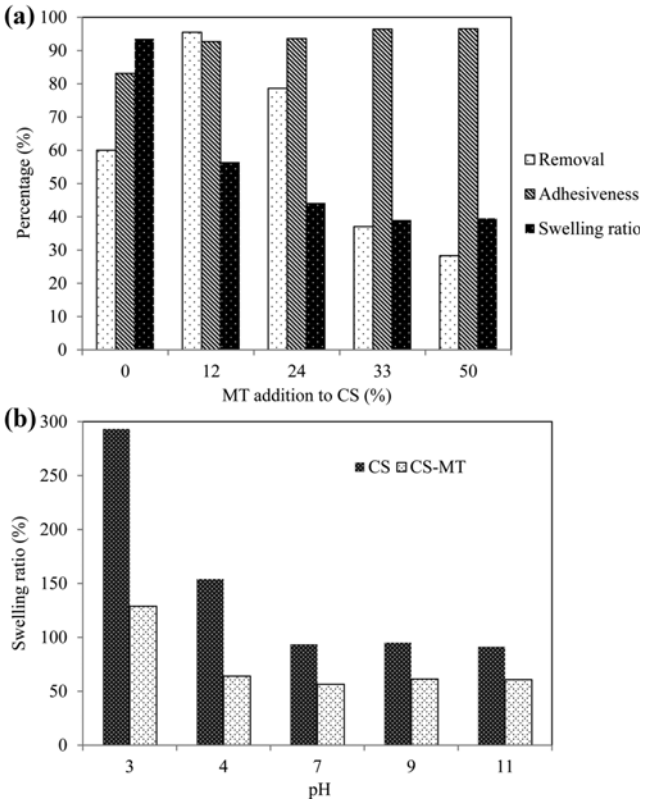

Fig. 1. (a) The removal efficiency of MO, adhesiveness and swelling ratio of immobilized CS-MT made from different MT clay composition casting solution and (b) the swelling ratio of CS-MT at different pH solutions (CS and CS-MT loading=1.3 mg cm^{-2}; $[MO]_o$=20 mg L^{-1}; pH=6.5; aeration flow rate=40 mL min^{-1}).

mer adsorbent plates that were prepared from the casting solution with 24%, 0%, 33% and 50% of MT composition. It was observed that the presence of 12% of MT within the CS-MT composite could remove MO better than the CS film only. However, excessive MT clay addition afterward could hinder the adsorption of MO by the protonated -NH_3^+ groups on the CS structure as the ratio of the positively charged adsorption sites of CS to the negatively charged MT on the adsorbent surface decreased. Thus, less MO could bind onto the positively charged adsorption sites, which decreased its removal efficiency. In the case of adhesiveness, CS could bind well on the glass plate as 84% of the polymer was still left after the mechanical test. However, further improvement was observed when MT clay was present within the immobilized composite adsorbent as the adhesiveness could reach 96%. The improvement was due to the uniform dispersion of MT clay particles within the CS matrix, but an excessive clay content could result in brittleness of the composite adsorbent [34,35]. A positive impact was also observed for swelling ratio (SR), which is an indicator for the water-holding capacity of polymeric films [34] as the value decreased significantly from 98% to 40% when more MT was present within the immobilized adsorbent. The results reflect that the CS-MT adsorbent was more stable than the CS adsorbent by itself and can possibly be applied in an aqueous medium. Similar results were also reported for alginate/MT [35] and potato starch/MT [36], which had shown better mechanical strength than their polymer counterpart. Based on the MO removal efficiency, adhesiveness and swelling tests studied, 12% of MT addition to CS was chosen as the optimum composition percentage.

Another swelling test was then performed using the optimum CS-MT plate in the pH-adjusted water solutions of pH 3 to 11 by referring to CS plate as seen in Fig. 1(b). It was observed that the SR values of the CS-MT plates were lower than the CS plates in all pH-adjusted solutions. A significant drop can be seen at pH 3 as the value of SR of CS-MT composite was reduced to more than half of that of CS. It has been known that CS easily dissolves in the acidic solution due to its protonated amine group and polar OH groups, which makes the polymer more hydrophilic. In case of CS-MT, the interaction of MT with the OH groups of CS left less free volume and less OH groups available for holding the water molecules, which eventually reduced the swelling of the composite film [34]. Similarly, for the other pH-adjusted solutions, a smaller number of OH groups remaining for CS-MT than CS film would result in the reduction of the SR value. From the observation on the adhesiveness and swelling ratio, it was proven that the presence of MT could enhance the physicochemical properties of CS-MT composite by improving the CS matrix's textures and its mechanical properties as well as reducing the swelling effect in every pH solution [37].

1-2. Surface Morphology

The SEM image of CS in Fig. 2(a) exhibits a smooth layer coating showing all CS particles dissolved completely in the acid solution and was distributed evenly on the supporting material. On the other hand, the CS-MT image in Fig. 2(b) shows that the MT clay was dispersed uniformly throughout the CS matrix without any distinct agglomeration. Apparently, both film images are free of visible pores or cracks and translucent even under high magnification. HRTEM analysis was then conducted to observe the spherical morphology of particles, which could not be seen under the SEM instrument. Figs. 2(c)-(d) show the HRTEM images of CS and CS-MT taken at 145,000 x magnifications. Under HRTEM, the particles of CS and CS-MT still look very tiny where their size ranges between 0.5-1 nm. The CS surface seems smooth and homogeneous, while the CS-MT exhibits a heterogeneous surface, indicating that the MT clay particles were well distributed throughout the polymer matrix. The SEM and HRTEM analyses support the adhesive test result that the uniformly distributed MT clay within the CS matrix improved the texture and strength of the composite on the glass support. The point of zero charges of CS and CS-MT as produced in this study is 6.3 and 6.5, respectively.

2. Thermal Stability

An analysis was done to observe the thermal stability of CS, MT and CS-MT in the range of 30-920 °C. In this case, the degradation temperature and final residual weight were investigated based on Fig. 3(a)-(b). The plots in Fig. 3(a) show that the CS and CS-MT underwent two stages of degradation, while it was only one stage for MT. The first degradation stage for all samples occurred in the range of 30-120 °C, from the loss of solvent such as water molecules. The weight loss exhibited by CS was the highest with 14.4%, followed by CS-MT (14.0%) and MT (2.5%). The second

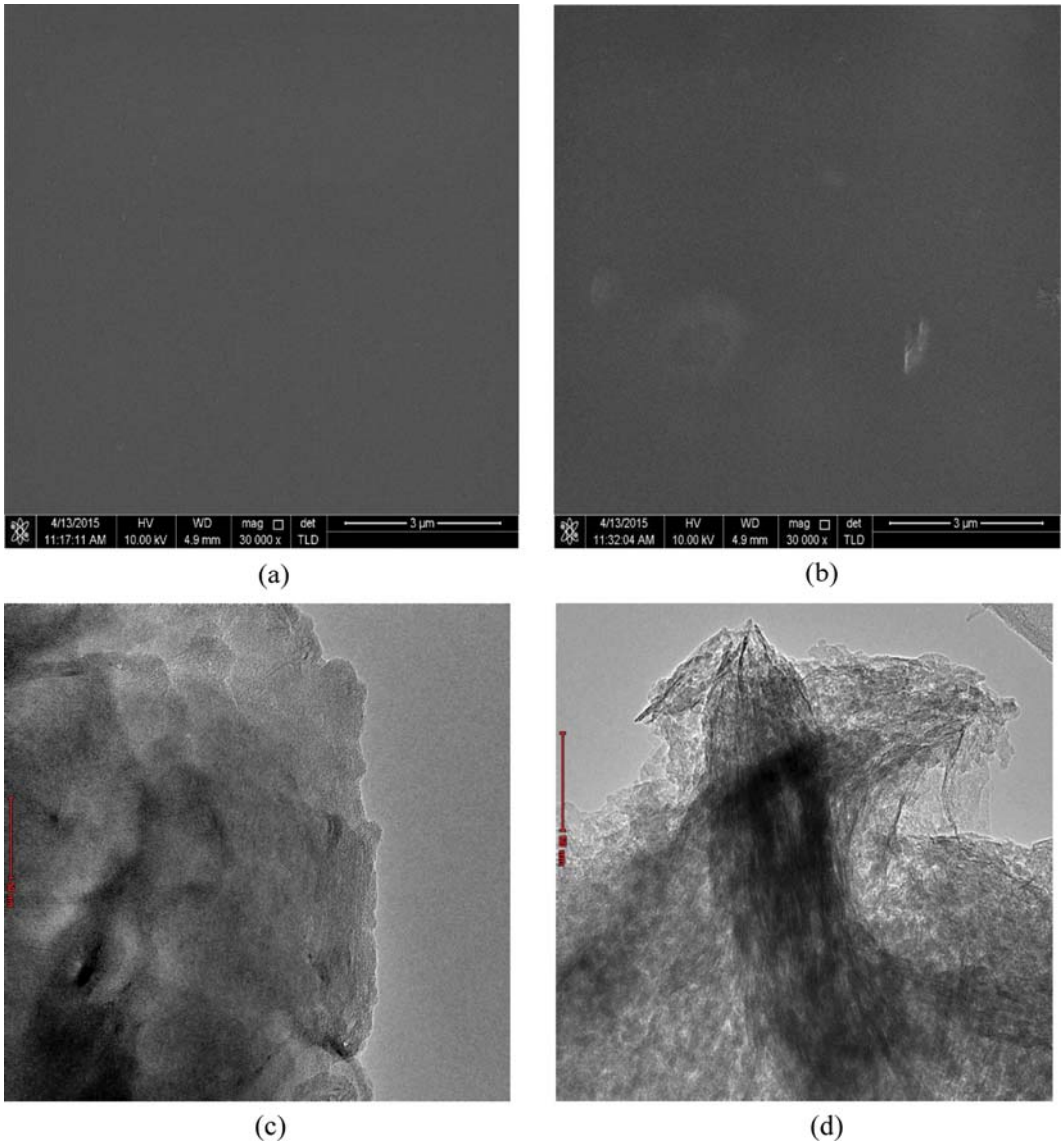

Fig. 2. Morphological images as observed using SEM ((a), (b)) at 30,000 x magnifications and HRTEM ((c), (d)) at 145,000 x magnifications of CS ((a), (c)) and CS-MT ((b), (d)).

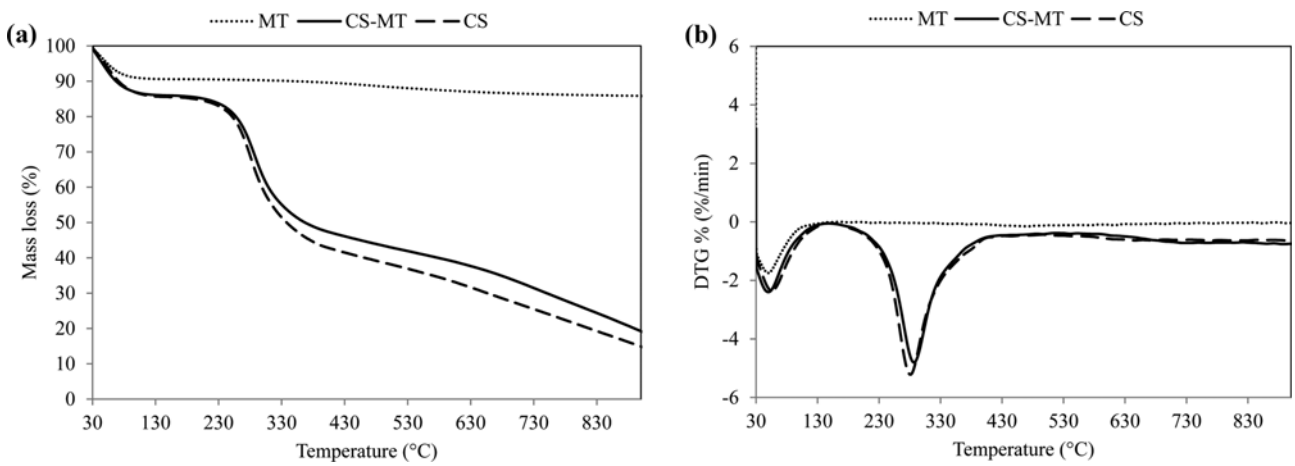

Fig. 3. (a) TGA and (b) DTG curves for MT, CS and CS-MT.

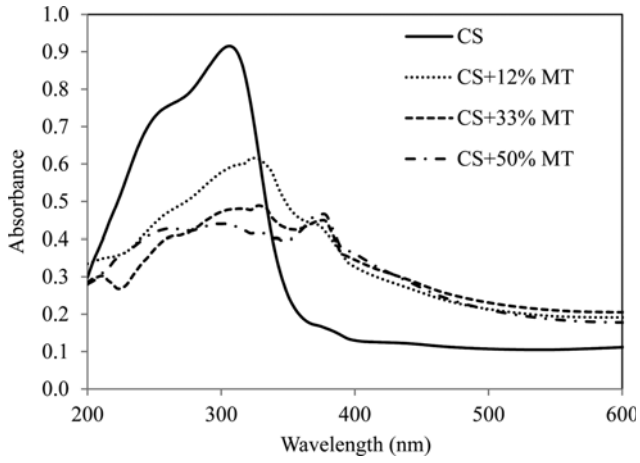

Fig. 4. UV-vis DRS spectra of CS and CS-MT composites of different MT clay percentage.

degradation stage temperature for CS and CS-MT is around 230-330 °C corresponding to the degradation and deacetylation of CS [38], whereby the residual samples left for CS and CS-MT were 13.9 and 18.0%, respectively. As expected, the presence of MT attributed to the thermal stability of CS-MT composite, whereby the final residue was 85.6% as compared to only 84.1% for CS. This proves that the presence of MT in the CS-MT composite could provide a thermal barrier and delay the weight loss of the composite [37,39].

3. Optical Characterizations

3-1. UV-vis Absorption

The effect of MT on the optical properties of the CS composite was further observed using a UV-vis diffuse reflectance spectroscopy. For the first analysis, only the adsorbent sub-layer was tested, which included CS and CS composites consisting of 12%, 33% and 50% of MT clay. As seen in Fig. 4, the absorbance of the photon in UV light region by CS only is the highest as compared to 12% of MT in the composite, followed by 33% and lastly by 50% of MT in composition. However, a contrasting result was observed for the visible light region in which all CS-MT composites absorbed the photon of longer wavelength than CS. That was likely because the thickness of MT layers is less than the wavelength of visible light; thus the clay layers do not divert light and are transparent [33]. According to the previous work on immobilized CS, the peak at 380 nm corresponds to the carbonyl group (C=O) on the CS backbone, which is an electron-withdrawing side group as a result of solid-state oxidation by TiO_2 photocatalyst [20]. The carbonyl group is responsible for the redshift response of CS-MT composite due to the primary $n \rightarrow \pi^*$ transition within the CS molecular structure [20,21]. The appearance of the peak in the as-prepared CS-MT composite in this study is probably due to the conversion of the CH_2OH group of CS to become the C=O group during the preparation of the CS-MT plates. That was likely attributed to the loss of water molecules within MT clay at 100 °C, which depleted the chemically bound OH group of MT as well as the hydrogen bonding between CS and MT [40-42]. For this case, the higher the percentage of clay is, the higher is the depletion of the OH groups, and thus the higher is the absorbance of the corresponding peak. Although the depletion of hydrogen bonding increased with the amount of clay, the strength of CS-MT composite on the support was not much affected as the amino group of CS could also bind to the OH groups of MT. However, the MO uptake would be lower as the positively charged binding sites would decrease as well. Among the composites, 12% of MT addition to CS shows the highest absorption in the UV region as well as comparable activity in visible light wavelength, thus was selected as the optimum composition percentage. The optical property findings corroborate well the observed physicochemical analyses for the optimum MT clay within the composite.

Table 2. Wavelength edge and band-gap energies of TiO_2, TiO_2/CS and TiO_2/CS-MT photocatalysts

Materials	Wavelength edge (nm)	Band-gap energy (eV)
TiO_2	406	3.02
TiO_2/CS	416	2.98
TiO_2/CS-MT	423	2.93

The UV-vis DRS analysis was then employed on the photocatalysts, namely, TiO_2/CS-MT, TiO_2/CS and TiO_2. From the results in Table 2, the absorption wavelength in the visible region for TiO_2/CS and TiO_2/CS-MT photocatalysts was enhanced at the edge of 416 and 423 nm, respectively, as compared to single TiO_2 at 406 nm. In this case, the observed visible light absorption of the bilayer photocatalysts is attributed to the interaction at the interface of the adsorbent and the TiO_2 surface where the two layers meet and mix in with a possibility of TiO_2 photosensitization by the adsorbent sub-layer [7]. High UV light absorption was also observed by potato starch/MT/TiO_2 nanocomposite than its counterparts due to the presence of empty orbital of Fe^{3+} in the structure of MT, which could absorb the energy photons [36]. Since CS-MT sub-layer absorbed the photon at a higher wavelength than CS, therefore, the TiO_2/CS-MT photocatalyst was likely to become more visible light active than the TiO_2/CS. Moreover, when the absorbance reading was converted to reflectance and fit into the Kubelka-Munk equation [32], the attained band gap energy of TiO_2/CS-MT was smaller than TiO_2/CS and TiO_2 as the corresponding band gap energy reduced to 2.93 eV for TiO_2/CS-MT and 2.98 for TiO_2/CS. The lower band gap energy for the TiO_2/CS-MT photocatalyst than the TiO_2/CS and single TiO_2 indicates that the former required less energy to initiate the electron excitation in TiO_2 as compared to the latter photocatalysts.

3-2. Detection of Hydroxyl Radicals

The improvement in the optical properties of TiO_2/CS photocatalyst in the presence of MT was furthered confirmed by fluorescence spectrophotometer analysis. The analysis can be used to determine the production of $^{\bullet}OH$ radicals using terephthalic acid (TA) during the photocatalytic oxidation [43]; the result of the analysis is shown in Fig. 5. The product of the reaction between TA solution and $^{\bullet}OH$ radicals is 2-hydroxy terephthalic acid (HTA), which appears at 425 nm and is directly proportional to the amount of $^{\bullet}OH$ radicals present in the solution. The highest fluorescence emission intensity was exhibited by the TiO_2/CS-MT photocatalyst, indicating the most production of the $^{\bullet}OH$ radicals, followed by TiO_2/CS and lastly, TiO_2. This high production of the $^{\bullet}OH$ radicals proves that they are the primary active species involved in the

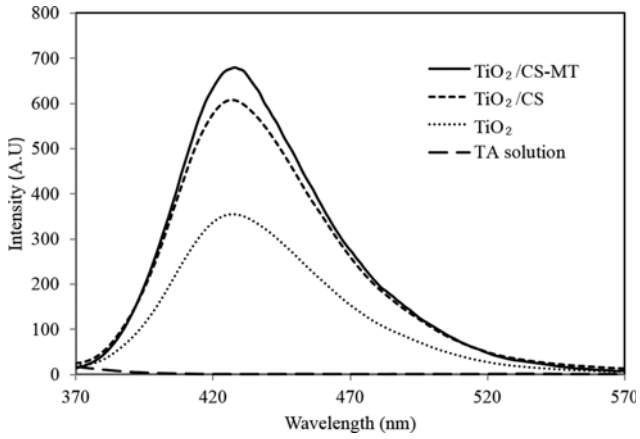

Fig. 5. Comparison of the individual photocatalysts in the TiO_2/CS-MT bilayer on the production of hydroxyl radicals ($^{\bullet}OH$) captured in TA solution (TiO_2 loading=2.5 mg cm^{-2}; CS and CS-MT loading=1.3 mg cm^{-2}; aeration flow rate=40 mL min^{-1}).

photocatalytic degradation. By comparing the intensity ratio, the production of $^{\bullet}OH$ radicals by TiO_2/CS-MT was 1.1 and 2.0-times better than TiO_2/CS and TiO_2, respectively. This is probably because the TiO_2/CS-MT photocatalyst could inhibit the recombination of electron-hole better than the other two photocatalysts; therefore, the separated electrons and holes could be used more effectively to produce the $^{\bullet}OH$ radicals. Eventually, the photocatalytic activity of TiO_2/CS-MT should be better than the other two photocatalysts as well.

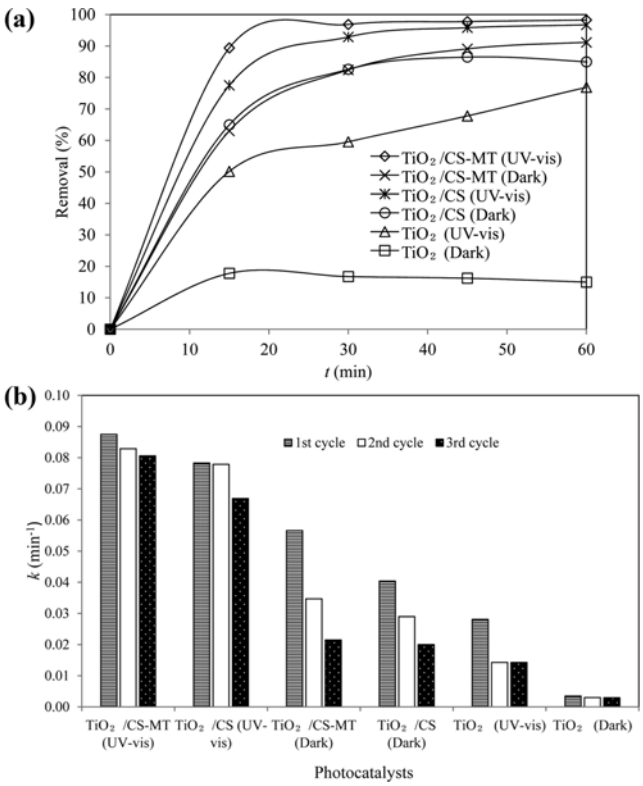

Fig. 6. (a) The removal efficiency and (b) pseudo-first-order rate constants of individual and bilayer photocatalysts for three cycles of application (TiO_2 loading=2.5 mg cm^{-2}; CS and CS-MT loading=1.3 mg cm^{-2}; $[MO]_o$=20 mg L^{-1}; pH=6.5; aeration flow rate=40 mL min^{-1}).

Table 3. Textural properties of CS and CS-MT composite

Properties	CS	CS-MT
BET surface area, S_{BET} (m^2g^{-1})	3.82	4.38
Pore volume, V_t (cm^3g^{-1})	0.081	0.076
Average pore diameter, D_{avg} (nm)	8.39	6.96

4. Photocatalytic Oxidation Performance

A performance comparison of the individual and the bilayer TiO_2/CS-MT photocatalysts is presented in Fig. 6(a) and (b) as a function of percentage removal and the rate constants for three cycles of treatment, respectively. It can be seen that the decolorization of MO by the TiO_2/CS-MT was the fastest when it was irradiated under light irradiation, which corresponded to 98.3% of MO removal. This was followed by TiO_2/CS under light irradiation with 96.7% of MO removal. On the other hand, 91.2 and 85.0% of MO was removed via sole adsorption in the dark by the TiO_2/CS-MT and TiO_2/CS, respectively. A better improvement in the removal efficiency was observed as exhibited by TiO_2/CS-MT via photocatalysis-adsorption and sole adsorption than the same processes by TiO_2/CS, most probably due to the increased S_{BET} value of the sub-layer of the former photocatalyst providing more adsorption sites as tabulated in Table 3. Obviously, the single TiO_2 layer showed the least removal of MO via photocatalytic process (76.9%) due to low dye adsorption on the photocatalyst surface, which was about 15.0%.

Fig. 6(b) shows the MO decolorization rate constant over three recycled applications of the individual and bilayer TiO_2/CS-MT photocatalysts. The removal of MO by the TiO_2/CS-MT via the photocatalysis-adsorption processes maintained the rate constant with only a slight reduction from 0.086 to 0.080 min^{-1} from the first to the third cycles. On the other hand, the rate constants by the TiO_2/CS via the same process were reduced from 0.078 to 0.067 min^{-1}. The adsorption of both TiO_2/CS-MT and TiO_2/CS photocatalysts show poor rate constants upon the consecutive cycles, which can be explained by the reduction in the adsorption sites of the photocatalysts due to the accumulation of unreacted MO dye from the previous cycle. Eventually, the amount of adsorbed MO would be decreased as well. The rate constants for single TiO_2 decreased significantly from 0.004 to 0.003 min^{-1} and 0.028 to 0.014 min^{-1} with the number of cycles via adsorption and photocatalysis process, respectively. It was observed that the TiO_2 bilayer arrangement with either CS or CS-MT sub-layer by the photocatalysis-adsorption processes showed the best removal due to the contribution from their adsorption properties of MO. However, the TiO_2/CS-MT photocatalyst is more suitable than the TiO_2/CS photocatalyst for water treatment application due to its improved physicochemical and optical properties as evidenced in previous sections.

5. Improving the Photocatalytic Activity of TiO_2/CS-MT

The instability of ENR during its modification with a peracid can contribute to the high carbon content leached out from the plates during the light irradiation. This was proven by Nawi and Zain [29] and Nawi et al. [44], who reported the degradation of ENR from TiO_2 layer upon irradiation by light which leached out

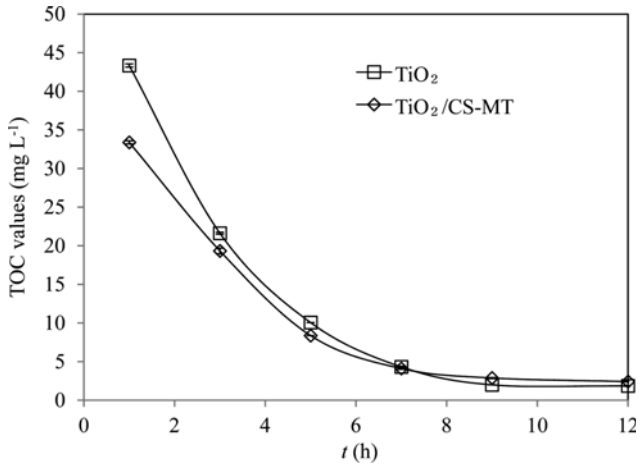

Fig. 7. TOC values during the photo-etching of TiO_2/CS-MT and TiO_2 photocatalysts for 12 hours of treatment (TiO_2 loading= 2.5 mg cm^{-2}; CS-MT loading=1.3 mg cm^{-2}; aeration flow rate= 40 mL min^{-1}).

into the solution in the form of dissolved organic matter (DOM). Interestingly, the degradation of ENR creates macropores within the TiO_2 surface that facilitates the penetration of light and oxidative radicals into the layers, increases the surface area and the photoactivity of the photocatalyst [20].

Fig. 7 shows the TOC values for the TiO_2/CS-MT and TiO_2 photocatalysts for 12 h of irradiation time. The initial TOC values for TiO_2/CS-MT and TiO_2 were 43.4 and 33.7 mg L^{-1}, respectively. High TOC values for TiO_2/CS-MT came from the degradation of ENR additive within the TiO_2 layer and CS of sub-layer which could compete with MO molecules for oxidative radicals and eventually slowed the photocatalytic activity. The values of TOC for both plates decreased with increasing irradiation time, indicating that the TiO_2 continuously oxidized the DOM in the treated solution. The TOC value for TiO_2/CS-MT and TiO_2 reached zero after 12 h of irradiation showing that the leached DOM from ENR degradation was

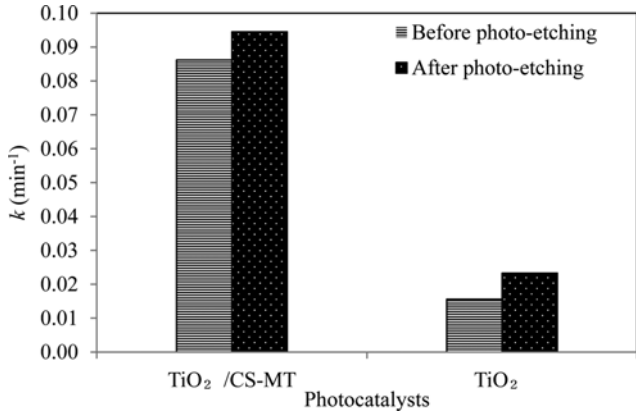

Fig. 8. Comparison of the pseudo-first-order rate constants of MO decolorization by TiO_2/CS-MT and TiO_2 photocatalysts before and after photo-etching (TiO_2 loading=2.5 mg cm^{-2}; CS-MT loading=1.3 mg cm^{-2}; $[MO]_o$=20 mg L^{-1}; pH=6.5; aeration flow rate=40 mL min^{-1}).

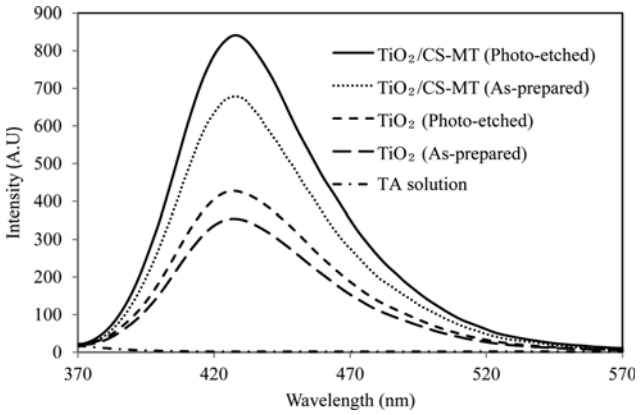

Fig. 9. Comparison of the production of hydroxyl radicals (•OH) as captured by TA in solution by as-prepared and photo-etched TiO_2/CS-MT photocatalyst (TiO_2 loading=2.5 mg cm^{-2}; CS-MT loading=1.3 mg cm^{-2}; aeration flow rate=40 mL min^{-1}).

oxidized completely and the polymer additive within TiO_2 had been stabilized. A comparison of the pseudo-first-order rate constant of the TiO_2/CS-MT and TiO_2 photocatalysts is depicted in Fig. 8. As seen, the rate constant significantly improved from 0.086 to 0.095 min^{-1} for TiO_2/CS-MT and 0.016 to 0.023 min^{-1} for TiO_2 after the photo-etching procedure. The reasons behind the improvement of the rate constants in MO decolorization after photo-etching were further investigated via FLS and UV-vis DRS analysis.

5-1. Production of Hydroxyl Radicals

The photocatalytic enhancement related to MO decolorization was observed by mean of the •OH radicals production by the TiO_2/CS-MT photocatalyst before and after photo-etching as seen in Fig. 9. The intensity of the fluorescence signal, which corresponded to the amount of •OH radicals produced by the photo-etched TiO_2/CS-MT and TiO_2 plates, was higher as compared to before the photo-etching was conducted. As mentioned, the photo-etching process eliminated interferences from the degradation of the polymer binder which could compete with the MO dye to consume the •OH radicals. The enhancement in the rate constant indicates the masking effect that obstructed the penetration of light photon to the as-prepared TiO_2 surface was eliminated, and this created the macropores within the TiO_2 surface. More photons could be adsorbed for the TiO_2 redox reaction, which allowed the separated charges to produce more hydroxyl radicals. Rapid recombination of active species could also have been inhibited, which eventually led to a better contact of the active radicals with MO molecules and induced better photoactivity of TiO_2 [7]. The generation of the macroporous TiO_2 surface can be referred to our previous works [5,9,44], while the increment in the radicals production after photo-etching was also observed for TiO_2/PANI [5].

5-2. Oxidation of CS within the CS-MT Composite

It has been demonstrated that the photo-etching process could also generate an oxidized CS film through •OH radicals attack of the functional group of CS backbone in the presence of TiO_2 top layer loading of more than 1.27 mg cm^{-2} [19]. The oxidation of CS film corresponds to the conversion of -CH_2OH group to the carbonyl functional group (C=O), which can enhance its physico-

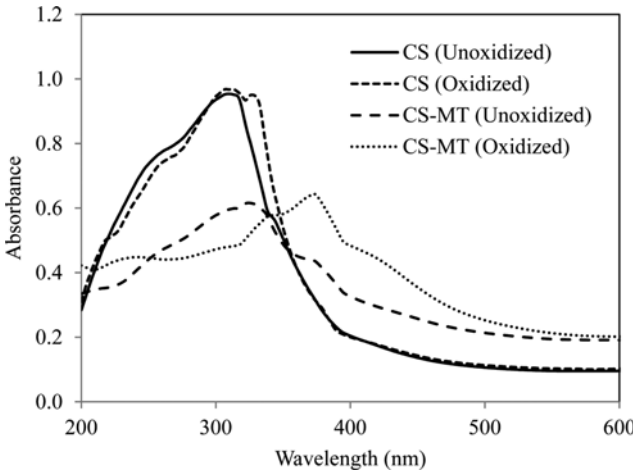

Fig. 10. UV-vis DRS spectra of the as-prepared and photo-etched CS and CS-MT after removing TiO_2 top layer.

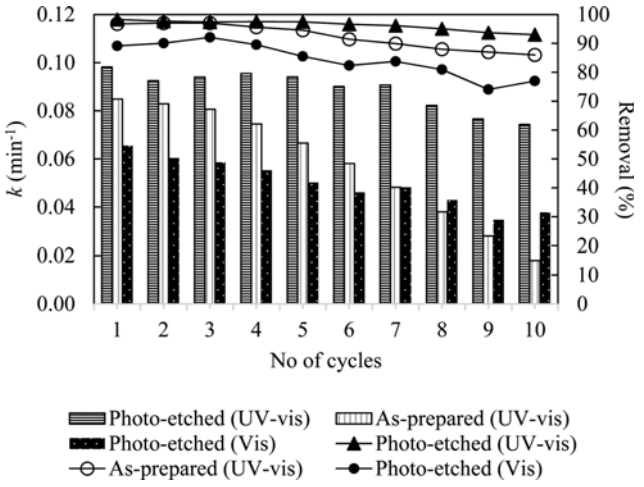

Fig. 11. The pseudo-first-order rate constant and removal efficiency of the as-prepared and photo-etched TiO_2/CS-MT photocatalyst under UV-vis and total visible light irradiation (TiO_2 loading=2.5 mg cm^{-2}; CS-MT loading=1.3 mg cm^{-2}; $[MO]_o$= 20 mg L^{-1}; pH=6.5; aeration flow rate=40 mL min^{-1}).

chemical and optical properties for multiple functionalities [21]. The effects of photo-etching and the presence of MT on the oxidation of CS of the TiO_2/CS-MT plate were further investigated by monitoring the optical changes before and after photo-etching using UV-vis DRS. The oxidized CS-MT sub-layer was obtained after removing the TiO_2 top layer using toluene after the photo-etching. A plate of TiO_2/CS was also included as a reference plate to observe the optical transformation of CS after the photo-etching.

As shown in Fig. 10, the original peak of CS before the photocatalytic oxidation was at 308 nm, which corresponded to $n\rightarrow\sigma^*$ transition of the amino group [19]. Apparently, the intensity of the amino peak dropped significantly when MT was added into the CS matrix due to the partial elimination of amino groups of CS which were bound to the OH groups of the clay. After the irradiation, the peak of oxidized CS-MT at 380 nm became more intense and the absorbance was higher as compared to the original peak corresponding to the rapid oxidation of the OH groups in the CS structure by the TiO_2 top layer and eventually produced the carbonyl group (C=O) on the CS backbone [19]. In addition, the decrease in the absorbance of the amino group after oxidation could be also due to the appearance of the carbonyl group [45]. The carbonyl side group (C=O) was ascribed to the transition of $n\rightarrow\pi^*$ of carboxyl and carbonyl group in CS [19]. Higher CS transformation was observed for the oxidized CS-MT than the CS plate since the oxidation process became more rapid due to higher production of $^{\bullet}OH$ radicals of the former plate after the photo-etching, as seen in Section 3.2 and Section 5.1. More $^{\bullet}OH$ radicals had possibly attacked the OH groups of CS and produced the C=O side groups, as high absorbance can be seen for 380 nm peak after the photo-etching. The surface transformation then induced the improvement of the overall photocatalytic activity of the bilayer photocatalyst, as observed earlier in Fig. 8. This mild photo-modification process produced a more chemically stable and optically active form of oxidized CS-MT without altering the composite polymeric structure [20].

6. Reusability

The ability of the as-prepared and photo-etched TiO_2/CS-MT plates to decolorize MO for ten repeated cycles was evaluated under UV-vis and total visible light irradiation based on the rate constant and removal efficiency as shown in Fig. 11. Less MO removed means more MO remained in the solution and vice versa. It can be observed that the photo-etched TiO_2/CS-MT photocatalyst shows the highest MO removal, followed by the as-prepared photocatalyst and photo-etched TiO_2/CS-MT under total visible light irradiation. The TiO_2/CS-MT photocatalyst under UV-vis light irradiation could constantly remove 95-100% of MO and exhibited an average constant of 0.09 min^{-1} throughout the ten cycles of application. This can be explained by the generation of the porous TiO_2 surface on the bilayer photocatalyst, which enabled the photons to reach out the CS-MT sub-layer surface and oxidized the CS structure and subsequently elevated the photocatalytic activity. Moreover, the porous TiO_2 surface would allow better diffusion of MO molecules to the deeper CS-MT layer for adsorption and improved the overall removal rate. In contrast, the as-prepared TiO_2/CS-MT photocatalyst removed MO efficiently by 95% for the first three cycles but started declining after the fourth cycle and onward with an average rate of 0.06 min^{-1} for all 10 cycles. This TiO_2/CS-MT photocatalyst could be saturated by the unoxidized MO molecules from the previous cycle due to its slow photocatalytic activity causing a decrement in the availability of free binding sites for the next cycles [46]. Meanwhile, the photocatalytic activity of photo-etched TiO_2/CS-MT under the visible light condition, which was closely related to the oxidized CS-MT sub-layer, followed a similar sustainability trend as under UV-vis irradiation but lower in photocatalytic activity with an average rate constant and removal of 0.050 min^{-1} and 84.5%, respectively for ten continuous cycles. Apparently, at the eighth cycle and onward, it preceded the rate of as-prepared photocatalyst under UV-vis lamp as the latter might be saturated with unoxidized MO molecules due its slow activity. Nevertheless, the reusability of TiO_2/CS-MT under UV-vis and visible light irradiation for repeated cycles indicates that this photocatalyst could pos-

sibly find its potential for indoor and outdoor applications.

CONCLUSIONS

The optimum percentage of MT addition to CS in the casting solution was 12%. The presence of MT enhanced the removal efficiency, swelling, adhesion strength as well as thermal stability of the CS-MT composite. Upon coating TiO_2 on the top of CS-MT layer, the photocatalytic activity of the photocatalyst was improved by 1.3 and 4.2-times than the TiO_2/CS and TiO_2 photocatalysts, respectively. The incorporation of CS-MT adsorbent under TiO_2 layer showed a redshift as the band gap energy was lowered to 2.93 eV and contributed to the most production of hydroxyl radicals as compared to the other photocatalysts. The effect of photoetching was pronounced, as better photocatalytic enhancement was observed due to increment in the hydroxyl radical production, while the oxidation of CS within the composite also improved in the presence of MT. The reusability of the TiO_2/CS-MT bilayer photocatalyst under total visible light irradiation was a promising result for real applications.

ACKNOWLEDGEMENT

The authors would like to acknowledge Universiti Sains Malaysia for providing the needed research facilities. All the research work in this article was funded by Malaysian Ministry of Education (MOE) through Fundamental Research Grant Scheme (FRGS) (203/PKIMIA/6711228). N.N Bahrudin would also like to thank MOE for granting MyPhD scholarship during her candidature.

REFERENCES

1. A. Ibhadon and P. Fitzpatrick, *Catalysts*, **3**, 189 (2013).
2. O. Omotunde, A. Okoronkwo, A. Aiyesanmi and E. Gurgur, *J. Photochem. Photobiol. A: Chem.*, **365**, 145 (2018).
3. R. R. Kalantary, Y. D. Shahamat, M. Farzadkia, A. Esrafili and H. Asgharnia, *Desalin. Water Treat.*, **55**, 555 (2015).
4. M. Nasirian and M. Mehrvar, *J. Env. Chem. Eng.*, **4**, 4072 (2016).
5. N. N. Bahrudin, M. A. Nawi and W. I. Nawawi, *Mater. Res. Bull.*, **106**, 388 (2018).
6. A. H. Jawad and M. A. Nawi, *React. Kinet. Mech. Cat.*, **106**, 49 (2012).
7. Y. S. Ngoh and M. A. Nawi, *Mater. Res. Bull.*, **76**, 8 (2016).
8. L. Yuan, D. Huang, W. Guo, Q. Yang and J. Yu, *Appl. Clay Sci.*, **53**, 272 (2011).
9. M. A. Nawi, A. H. Jawad, S. Sabar and W. S. W. Ngah, *Desalination*, **280**, 288 (2011).
10. R. Zhu, Q. Chen, Q. Zhou, Y. Xi, J. Zhu and H. He, *Appl. Clay Sci.*, **123**, 239 (2016).
11. D. Chen, H. Zhu and X. Wang, *Appl. Surf. Sci.*, **319**, 158 (2014).
12. J. Gillott, *Clay Miner.*, **21**, 261 (1986).
13. H. Wang, H. Tang, Z. Liu, X. Zhang, Z. Hao and Z. Liu, *J. Environ. Sci.*, **26**, 1879 (2014).
14. M. A. Nawi, S. Sabar and Sheilatina, *J. Colloid Interface Sci.*, **372**, 80 (2012).
15. A. R. Nesic, S. J. Velickovic and D. G. Antonovic, *J. Hazard. Mater.*, **209**, 256 (2012).
16. R. Celis, M. Adelino, M. Hermosín and J. Cornejo, *J. Hazard. Mater.*, **209**, 67 (2012).
17. T. Kamal, Y. Anwar, S. B. Khan, M. T. S. Chani and A. M. Asiri, *Carbohydr. Polym.*, **148**, 153 (2016).
18. S. Sabar and M. A. Nawi, *Desalin. Water Treat.*, **57**, 10312 (2016).
19. M. A. Nawi, A. H. Jawad, S. Sabar and W. S. W. Ngah, *Carbohydr. Polym.*, **83**, 1146 (2011).
20. A. H. Jawad and M. A. Nawi, *J. Polym. Environ.*, **20**, 817 (2012).
21. A. H. Jawad and M. Nawi, *Carbohydr. Polym.*, **90**, 87 (2012).
22. M. Tahir and N. S. Amin, *Appl. Catal., B*, **142-143**, 512 (2013).
23. H. Yan, H. Yang, A. Li and R. Cheng, *Chem. Eng. J.*, **284**, 1397 (2016).
24. T. Zhang, Y. Luo, B. Jia, Y. Li, L. Yuan and J. Yu, *J. Environ. Sci.*, **32**, 108 (2015).
25. B. Dou, V. Dupont, W. Pan and B. Chen, *Chem. Eng. J.*, **166**, 631 (2011).
26. V. Vijayalekshmi, *Res. J. Recent Sci.*, **2277**, 2502 (2015).
27. N. N. Bahrudin and M. A. Nawi, *React. Kinet. Mech. Cat.*, **124**, 153 (2018).
28. N. N. Bahrudin and M. A. Nawi, *Korean J. Chem. Eng.*, **35**, 1532 (2018).
29. M. A. Nawi and S. M. Zain, *Appl. Surf. Sci.*, **258**, 6148 (2012).
30. S. Razak, M. A. Nawi and K. Haitham, *Appl. Surf. Sci.*, **319**, 90 (2014).
31. Y. Wan, K. A. M. Creber, B. Peppley and V. T. Bui, *J. Appl. Polym. Sci.*, **89**, 306 (2003).
32. N. A. Sabri, M. A. Nawi and W. I. Nawawi, *Opt. Mater.*, **48**, 258 (2015).
33. M. V. Dias, V. M. Azevedo, S. V. Borges, N. d. F. F. Soares, R. V. de Barros Fernandes, J. J. Marques and É. A. A. Medeiros, *Food Chem.*, **165**, 323 (2014).
34. G. Liu, Y. Song, J. Wang, H. Zhuang, L. Ma, C. Li, Y. Liu and J. Zhang, *LWT-Food Sci. Technol.*, **57**, 562 (2014).
35. M. Alboofetileh, M. Rezaei, H. Hosseini and M. Abdollahi, *J. Food Eng.*, **117**, 26 (2013).
36. S. A. Oleyaei, H. Almasi, B. Ghanbarzadeh and A. A. Moayedi, *Carbohydr. Polym.*, **152**, 253 (2016).
37. Z. Shou, H. Le, S. Qu, R. Rothwell and R. Mackay, *Key Eng. Mater.*, **512**, 1746 (2012).
38. S. Wang, L. Shen, Y. Tong, L. Chen, I. Phang, P. Lim and T. Liu, *Polym. Degrad. Stab.*, **90**, 123 (2005).
39. K. S. Katti, D. R. Katti and R. Dash, *Biomed. Mater.*, **3**, 034122 (2008).
40. Q. Sun, W. Zhang and H. Qian, *Environ. Earth Sci.*, **75**, 610 (2016).
41. M. A. Nawi, A. H. Jawad, S. Sabar and W. S. W. Ngah, *Carbohydr. Polym.*, **83**, 1146 (2011).
42. F. A. R. Pereira, K. S. Sousa, G. R. S. Cavalcanti, M. G. Fonseca, A. G. de Souza and A. P. M. Alves, *Int. J. Biol. Macromol.*, **61**, 471 (2013).
43. Y. Nakabayashi and Y. Nosaka, *Phys. Chem. Chem. Phys.*, **17**, 30570 (2015).
44. M. A. Nawi, Y. S. Ngoh and S. M. Zain, *Int. J. Photoenergy*, **2012**, 12 (2012).
45. M. Mucha and A. Pawlak, *Polimery*, **47**, 509 (2002).
46. N. N. Bahrudin, M. A. Nawi and W. I. Nawawi, *Korean J. Chem. Eng.*, **35**, 1450 (2018).

47. X. Zhang, G. Xiao, Y. Wang, Y. Zhao, H. Su and T. Tan, *Carbohydr. Polym.*, **169**, 101 (2017).
48. J. Balaji and M. Sethuraman, *Int. J. Biol. Macromol.*, **104**, 1730 (2017).
49. H. Sun, T. Peng, B. Liu and H. Xian, *Appl. Clay Sci.*, **114**, 440 (2015).
50. K. Bahranowski, A. Gaweł, A. Klimek, A. Michalik-Zym, B. Napruszewska, M. Nattich-Rak, M. Rogowska and E. Serwicka, *Appl. Clay Sci.*, **140**, 75 (2017).